

Optimal Precoders for Tracking the AoD and AoA of a mmWave Path

Nil Garcia, Henk Wymeersch, Dirk Slock

Abstract—Due to high penetration losses, millimeter wave channels are formed of few paths. Most channel estimation procedures exploit this property by sounding the channel in multiple directions and then identifying those yielding the largest power. Whether in initial access or tracking mode, the beams for sweeping the channel have maximum gain towards a small range of angles. These beams are generally heuristic in nature and may not lead to the best estimation/tracking performance. In this paper, we derive optimal precoders for estimating the parameters of a single path, when prior knowledge is available, according to the Cramér-Rao lower bound.

I. INTRODUCTION

MILLIMETER-WAVE (mmWave) communication is expected to be one of the key enablers of 5th generation cellular networks [1]. Operating in mmWave frequencies offers a few advantages. First, there are large portions of underutilized bandwidth which could be used for multi-gigabit communications [2]. Second, an advantage of operating at higher carrier frequencies (30 GHz and above) than previous legacy systems is that, due to the much shorter wavelength, MIMO systems consisting of many antennas can be compacted into much smaller sizes. However, in order to compensate for the stringent path losses characteristic of millimeter wave, highly directional beamforming is necessary at the transmitter and/or receiver [3]. Since beamforming can only be achieved after learning the channel, it is critical that precise fast channel estimation techniques are developed.

Due to the high penetration losses at mmWave frequencies, the channel can be considered parsimonious in the sense that only a few multipath components carry non-negligible energy [4], [5]. This structure inherent to the mmWave channel is leveraged in many works for performing quicker and/or finer channel estimation [6]–[10]. Depending on whether channel state information (CSI) is available, the channel estimation techniques can be categorized in (a) initial access, or (b) tracking. Typically, the output of initial access is a set of angle-of-departures (AoD), angle-of-arrivals (AoA) and channel gains of the individual paths. Due to the mobility of the users and the variability of the environment [11], [12], the validity of the initial access estimates come with an expiration time, and so it is necessary to estimate/track the channel periodically. The main idea behind tracking is that CSI is carried over to the

next iteration, thus increasing the channel estimation accuracy and/or reducing the channel estimation overhead [13]–[16]. In this type of geometric models, the channel parameters can be linked to the environment, and so in location-aware communications, CSI may also be obtained through extraneous positioning and sensing technologies such as GPS, radars, cameras, etcetera [12], [17]. For instance, if prior knowledge on the user position is available through GPS, then the set of possible directions between the base station and the user can be considerably narrowed [18]–[20].

Whether initial access or tracking, the most common procedure for estimating the mmWave channel consists in sweeping the channel with directional beams at the transmitter and/or receiver [8], [21], [22]. By detecting the time at which the received power is the largest, the correct pair of beams can be identified and the AoD and/or AoA estimated for each path. While intuitive, such beams may not necessarily yield the best achievable estimation accuracy. To the best of our knowledge, the literature in mmWave precoding has not addressed what are the fundamental limits in terms of AoA and AoD estimation when performing *optimal precoding* at the transmitter.

In this work, we seek to find the best transmit precoders for estimating the AoD and AoA, for a single-path channel, assuming that the AoD and AoA are known to lie within some ranges of angles. Coarse knowledge on the AoD/AoA (CSI) may be available, for instance, through initial access; or alternatively, they may correspond to previous AoD/AoA estimates blurred over time due to the mobility of the user. The benefit of knowing that the AoD and AoA are constraint to a subset of angles is that the channel estimation duration can be substantially reduced, and the received SNR can be increased by highly directional beamforming. In fact, according to [23], the higher path loss of the mmWave channel in comparison to microwave frequencies can be fully compensated through beamforming. To abstract the analysis from specific estimators, we use the Cramér-Rao bound (CRB) from [24] as a proxy metric for the variance of the AoD and AoA. Indeed, the CRB is a lower-bound on the variance of any unbiased estimator and it is tight at high-SNR under some mild conditions [25]. The main contributions are

- Novel formulation of the optimal precoders according to the CRB on the AoD/AoA, with the option to include array gain constraints.
- Global optimization of the proposed non-convex problems by leveraging tools of convex optimization and majorization theory.
- Qualitative interpretation of the CRB expressions, and analysis of the optimal beampatterns.

N. Garcia and H. Wymeersch are with the Department of Signals and Systems, Chalmers University of Technology, Gothenburg, Sweden. D. Slock is with the Department of Communication Systems, EURECOM, Biot, France. This research was supported in part, by the EU HIGHTS project (High precision positioning for cooperative ITS applications) MG-3.5a-2014-636537, the VINNOVA COPPLAR project, funded under Strategic Vehicle Research and Innovation grant No. 2015-04849.

The remainder of this paper is organized as follows. In Section II the system model and problem are described. Section III contains the formulation of the proposed precoders as well as the solution strategy and different extensions. Numerical results are presented in Section IV, followed by conclusions in Section V.

II. SYSTEM MODEL

Assume a transmitter (Tx) and a receiver (Rx) with N_{Tx} and N_{Rx} antennas, respectively. The Tx sends M consecutive training sequences (or pilots) consisting of K symbols, each, precoded by the weigh vectors $\mathbf{f}_1, \dots, \mathbf{f}_M \in \mathbb{C}^{N_{\text{Tx}} \times 1}$. In arrays with large number of antennas, it is prohibitive to have a radio-frequency (RF) chain for each antenna, and so a common approach is to perform some sort of analog combining at the Rx in order to reduce the dimension of the received signals. Let L be the number of RF chains at the Rx, then the received snapshot for the k -th symbol of the m -th training sequence after combining and baseband conversion is

$$\mathbf{y}_{m,k} = \mathbf{W}^H (\mathbf{H} \mathbf{f}_m s_k + \mathbf{n}_{m,k}), \quad (1)$$

where $\mathbf{W} \in \mathbb{C}^{N_{\text{Rx}} \times L}$ is the combining matrix, $\mathbf{H} \in \mathbb{C}^{N_{\text{Rx}} \times N_{\text{Tx}}}$ is the channel matrix, and $\mathbf{n}_{m,k} \sim \mathcal{CN}(\mathbf{0}, \sigma^2 \mathbf{I})$ is white Gaussian noise. Without loss of generality the precoders and combiners are normalized to unit-norm. Let $\mathbf{a}_{\text{Tx}}(\theta) \in \mathbb{C}^{N_{\text{Tx}} \times 1}$ and $\mathbf{a}_{\text{Rx}}(\phi) \in \mathbb{C}^{N_{\text{Rx}} \times 1}$ be the array responses of the Tx and Rx, respectively. We will further assume to operate in a channel tracking mode [26]–[28], so that the combiner and precoder have spatially filtered the dominant propagation path. In that case, the MIMO channel matrix effectively becomes

$$\mathbf{H} = \alpha \mathbf{a}_{\text{Rx}}(\phi) \mathbf{a}_{\text{Tx}}^H(\theta), \quad (2)$$

where α , ϕ , θ are the channel gain, AoA, AoD, respectively. Here, the implicit assumption is the bandwidth of the signal is much smaller than the carrier frequency, so that the array responses are independent of the frequency. Coherently aggregating the symbols of each training sequence results in

$$\mathbf{y}_m = \sum_{k=1}^K s_k^* \mathbf{y}_{m,k} = \mathbf{W}^H \left(\mathbf{H} \mathbf{f}_m + \sum_{k=1}^K s_k^* \mathbf{n}_{m,k} \right), \quad (3)$$

where $\mathbf{s} = [s_1, \dots, s_K]$. Finally, by stacking $\mathbf{y}_1, \dots, \mathbf{y}_M$ as column vectors and dividing by $\|\mathbf{s}\|_2$, we reach the following matrix form for our signal model:

$$\mathbf{Y} = \frac{1}{\|\mathbf{s}\|_2} [\mathbf{y}_1 \quad \dots \quad \mathbf{y}_M] = \|\mathbf{s}\|_2 \mathbf{W}^H \mathbf{H} \mathbf{F} + \mathbf{N} \quad (4)$$

where $\mathbf{F} = [\mathbf{f}_1 \dots \mathbf{f}_M]$ and, because the columns of \mathbf{W} are assumed to be orthogonal, the components of \mathbf{N} are i.i.d. Gaussian variables with variance σ^2 . To assume that the columns of \mathbf{W} are orthogonal is reasonable; for instance, this would be the case of an array of subarrays where each RF chain is routed to a disjoint subset of antennas [29]. Another strategy leading to the same signal model is one where for each precoder, the Rx testes L different combiners successively in time [6].

It is our objective to find the optimal precoders \mathbf{F} that maximize the quality of the channel estimate, given no knowledge

of the channel gain, but assuming that the AoD and AoA are known to be within a small range of angles¹: $\theta \in \mathcal{R}_{\text{Tx}}$ and $\phi \in \mathcal{R}_{\text{Rx}}$. These ranges represent a priori uncertainty regarding the AoD/AoA, originating from mobility of the receiver, or from uncertainty in the tracking algorithm, or from uncertainty in location-aided communications [18]–[20]. We tackle this problem by optimizing the precoders in terms of the CRB² on the AoD and/or AoA.

III. OPTIMAL PRECODERS

To design the precoders, we choose as metric the CRB, which is a lower-bound on the variance of any unbiased estimator. Such bound is well suited to this problem because it generally leads to tractable mathematical expressions, and more importantly, for a sufficient large SNR and under some mild conditions [25], the variance of the maximum likelihood estimator (MLE) is tight to the CRB. If θ and ϕ are the AoD and AoA, respectively, of the LOS path, then determining θ yields the direction from the Tx to the Rx, and determining ϕ provides the Rx's orientation with respect to the Tx. Thus, for naming purposes and without loss of generality, we refer to the CRB on the θ as direction error bound (DEB), and the CRB on ϕ as orientation error bound (OEB). Once the DEB and OEB are derived, we will proceed with the optimization of the precoder.

A. Derivation of the DEB and OEB

From Appendix A, the direction error bound is

$$\text{var}(\hat{\theta}) \geq \text{DEB} = \left[2 \text{SNR} \|\mathbf{W}^H \mathbf{a}_{\text{Rx}}(\phi)\|_2^2 \left(\|\mathbf{F}^H \dot{\mathbf{a}}_{\text{Tx}}(\theta)\|_2^2 - \frac{|\mathbf{a}_{\text{Tx}}^H(\theta) \mathbf{F} \mathbf{F}^H \dot{\mathbf{a}}_{\text{Tx}}(\theta)|^2}{\|\mathbf{F}^H \mathbf{a}_{\text{Tx}}(\theta)\|_2^2} \right) \right]^{-1}, \quad (5)$$

and the orientation error bound is

$$\text{var}(\hat{\phi}) \geq \text{OEB} = \left[2 \text{SNR} \|\mathbf{F}^H \mathbf{a}_{\text{Tx}}(\theta)\|_2^2 \left(\|\mathbf{W}^H \dot{\mathbf{a}}_{\text{Rx}}(\phi)\|_2^2 - \frac{|\mathbf{a}_{\text{Rx}}^H(\phi) \mathbf{W} \mathbf{W}^H \dot{\mathbf{a}}_{\text{Rx}}(\phi)|^2}{\|\mathbf{W}^H \mathbf{a}_{\text{Rx}}(\phi)\|_2^2} \right) \right]^{-1}, \quad (6)$$

where $\dot{\mathbf{a}}_{\text{Tx}}(\theta) \triangleq \frac{d\mathbf{a}_{\text{Tx}}(\theta)}{d\theta}$, $\dot{\mathbf{a}}_{\text{Rx}}(\phi) \triangleq \frac{d\mathbf{a}_{\text{Rx}}(\phi)}{d\phi}$ and

$$\text{SNR} \triangleq \frac{|\alpha|^2 \|\mathbf{s}\|_2^2}{\sigma^2}. \quad (7)$$

Interpretation for the OEB: Define the array gain at the Tx as

$$g(\theta, \mathbf{f}_m) \triangleq |\mathbf{f}_m^H \mathbf{a}_{\text{Tx}}(\theta)|, \quad (8)$$

¹If the prior distributions of the AoD/AoA are provided instead, these ranges may be obtained from the confidence intervals.

²The use of the CRB requires a high-SNR operating condition. While mmWave communication operates under low SNR without beamforming [23], our tracking scenario is congruent with a medium-to-high SNR assumption.

and the aggregated gain (which is the equivalent gain at the receiver if the energy of the M training sequences is coherently combined) as

$$g_T(\theta, \mathbf{F}) \triangleq \sqrt{\sum_{m=1}^M |g(\theta, \mathbf{f}_m)|^2} = \|\mathbf{F}^H \mathbf{a}_{Tx}(\theta)\|_2. \quad (9)$$

From the transmitter's perspective, minimizing the OEB boils down to maximizing the aggregated array gain towards direction $\|\mathbf{F}^H \mathbf{a}_{Tx}(\theta)\|_2^2$, which makes sense because maximizing the received energy helps combat the noise.

Interpretation for the DEB: The intuition behind DEB's expression is a bit more cumbersome since it includes multiple terms that depend on \mathbf{F} . For notation convenience, define $\mathbf{s}(\theta, \mathbf{F}) \triangleq \mathbf{F}^H \mathbf{a}_{Tx}(\theta)$ and its derivative $\dot{\mathbf{s}}(\theta, \mathbf{F}) \triangleq \frac{d}{d\theta} \mathbf{s}(\theta, \mathbf{F})$. By omitting all factors that do not depend on \mathbf{F} , the DEB may be expressed as

$$\text{DEB} \propto \left(\|\dot{\mathbf{s}}(\theta, \mathbf{F})\|_2^2 - \left| \frac{\mathbf{s}^H(\theta, \mathbf{F})}{\|\mathbf{s}(\theta, \mathbf{F})\|_2} \dot{\mathbf{s}}(\theta, \mathbf{F}) \right|^2 \right)^{-1} \quad (10)$$

$$= \|\dot{\mathbf{s}}_{\perp}(\theta, \mathbf{F})\|_2^{-2}, \quad (11)$$

where $\dot{\mathbf{s}}_{\perp}(\theta, \mathbf{F})$ is the projection of $\dot{\mathbf{s}}(\theta, \mathbf{F})$ onto the orthogonal complement of $\mathbf{s}(\theta, \mathbf{F})$. The function $\mathbf{s}(\theta, \mathbf{F})$ not only appears in the CRB, but careful attention reveals that it also appears in the signal model (2), (4),

$$\mathbf{Y} = \alpha \|\mathbf{s}\|_2 \mathbf{W}^H \mathbf{a}_{Rx}(\phi) \mathbf{s}^H(\theta, \mathbf{F}) + \mathbf{N}, \quad (12)$$

and it carries all information about the AoD. Since the CRB is a tight lower bound on the variance when the noise tends to zero, the signal $\mathbf{s}(\theta, \mathbf{F})$ should be analyzed for the case where a small perturbation is applied to the AoD, in which case a good approximation is its first order Taylor polynomial

$$\mathbf{s}(\theta', \mathbf{F}) \approx \mathbf{s}(\theta, \mathbf{F}) + (\theta' - \theta) \dot{\mathbf{s}}(\theta, \mathbf{F}), \quad (13)$$

where θ' and θ represent two closely spaced AoD. Let $\beta \mathbf{s}(\theta, \mathbf{F})$ be the projection of $\dot{\mathbf{s}}(\theta, \mathbf{F})$ onto $\mathbf{s}(\theta, \mathbf{F})$, then,

$$\mathbf{s}(\theta', \mathbf{F}) \approx [1 + (\theta' - \theta)\beta] \mathbf{s}(\theta, \mathbf{F}) + (\theta' - \theta) \dot{\mathbf{s}}_{\perp}(\theta, \mathbf{F}). \quad (14)$$

From (13) we can infer that if $\dot{\mathbf{s}}(\theta, \mathbf{F})$ is large, $\mathbf{s}(\theta', \mathbf{F})$ and $\mathbf{s}(\theta, \mathbf{F})$ will differ more. However, from (14) if $\dot{\mathbf{s}}(\theta, \mathbf{F})$ is simply a scaled copy of $\mathbf{s}(\theta, \mathbf{F})$, then $\dot{\mathbf{s}}_{\perp}(\theta, \mathbf{F}) = 0$ and the two signals will only differ in a scaling constant. Since the channel gains are unknown, two proportional signals will be indistinguishable, and therefore, the AoD will not be correctly estimated. Thus, as asserted by the DEB, the accuracy in estimating the AoD depends on the magnitude of the part of $\dot{\mathbf{s}}(\theta, \mathbf{F})$ orthogonal to $\mathbf{s}(\theta, \mathbf{F})$.

Remark – CRB for Multipath Channels: When the combiner and precoders illuminate multiple paths, we must consider a multipath channel with L paths, i.e., $\mathbf{H} = \sum_{l=1}^L \alpha_l \mathbf{a}_{Rx}(\phi_l) \mathbf{a}_{Tx}^H(\theta_l)$ instead of (2). Computing the CRB on the unknown parameters of L paths is challenging because it would require inverting the Fisher information matrix (FIM, Section A), whose size grows quadratically with the number of paths. However, if the signals associated to all paths were pairwise orthogonal, then the FIM would become block diagonal and the CRB would boil down to inverting the FIM for each

individual path. The signal orthogonality condition is accurate if the AoAs are sufficiently apart from each other [30].

B. Problem Formulation

Both lower-bounds depend on the precoders \mathbf{F} , but also on the AoD θ and AoA ϕ which are unknown. Next, we propose a robust or min-max approach to the precoders design problem:

Problem 1. *AoD-AoA-optimal precoders.* Find the precoders that minimize the worst case DEB or OEB for all possible values of the AoD and AoA.

$$\min_{\|\mathbf{f}_m\|_2=1, m=1, \dots, M} \max_{(\theta, \phi) \in \mathcal{R}_{Tx} \times \mathcal{R}_{Rx}} \max \{DEB, OEB\} \quad (15)$$

The dependence of the DEB and OEB on θ , ϕ and \mathbf{F} has been omitted for notation clarity. Alternatively, if the only parameter of interest is the AoD, the optimal precoders are the solution to:

Problem 2. *AoD-optimal precoders.* Find the precoders that minimize the worst case DEB for all possible values of the AoD and AoA.

$$\min_{\|\mathbf{f}_m\|_2=1, m=1, \dots, M} \max_{(\theta, \phi) \in \mathcal{R}_{Tx} \times \mathcal{R}_{Rx}} DEB \quad (16)$$

Conversely, if the only parameter of interest is the AoA, the optimal precoders are obtained from:

Problem 3. *AoA-optimal precoders.* Find the precoders that minimize the worst case OEB for all possible values of the AoD and AoA.

$$\min_{\|\mathbf{f}_m\|_2=1, m=1, \dots, M} \max_{(\theta, \phi) \in \mathcal{R}_{Tx} \times \mathcal{R}_{Rx}} OEB \quad (17)$$

C. Convex Reformulation

Problems 1 to 3 are non-convex (with respect to \mathbf{F}), and therefore, computing their global minimum efficiently is challenging. For a proof of non-convexity, note that the OEB is concave because it is proportional to $\|\mathbf{F}^H \mathbf{a}_{Tx}(\theta)\|^{-2}$, and the DEB depends on the concave term $\|\mathbf{F}^H \dot{\mathbf{a}}_{Tx}(\theta)\|^{-2}$. In this section, Problems 1 to 3 will be reformulated as conic optimization problems, which is a subclass of convex problems. The conditions upon which the original problems and their convex reformulations are equivalent (in the sense that yields the same solution) will be analyzed in the next section.

The analysis focuses in Problem 1 because the solutions to Problems 2 and 3 will be shown to be subcases. An equivalent optimization problem to Problem 1 is

$$\max_{\|\mathbf{f}_m\|_2=1, m=1, \dots, M} \min_{(\theta, \phi) \in \mathcal{R}_{Tx} \times \mathcal{R}_{Rx}} \min \{DEB^{-1}, OEB^{-1}\} \quad (18)$$

because $f(x) = x^{-1}$ is a strictly decreasing function for $x > 0$. By introducing a slack variable t , the above problem can be expressed in the hypograph form:

$$\max_{\mathbf{F}, t} t \quad (19a)$$

$$\text{s.t.} \quad \min_{(\theta, \phi) \in \mathcal{R}_{\text{Tx}} \times \mathcal{R}_{\text{Rx}}} \text{DEB}^{-1} \geq t \quad (19b)$$

$$\min_{(\theta, \phi) \in \mathcal{R}_{\text{Tx}} \times \mathcal{R}_{\text{Rx}}} \text{OEB}^{-1} \geq t \quad (19c)$$

$$\|\mathbf{f}_m\|_2 = 1 \quad m = 1, \dots, M. \quad (19d)$$

Grid Approximation: The continuous set $\mathcal{R}_{\text{Tx}} \times \mathcal{R}_{\text{Rx}}$ makes optimizing over constraints (19b)–(19c) challenging. Instead we approximate it by a grid $\tilde{\mathcal{R}}_{\text{Tx}} \times \tilde{\mathcal{R}}_{\text{Rx}}$ such that

$$\tilde{\mathcal{R}}_{\text{Tx}} = \{\vartheta^1, \dots, \vartheta^{S_{\text{Tx}}}\} \subset \mathcal{R}_{\text{Tx}} \quad (20)$$

$$\tilde{\mathcal{R}}_{\text{Rx}} = \{\varphi^1, \dots, \varphi^{S_{\text{Rx}}}\} \subset \mathcal{R}_{\text{Rx}}, \quad (21)$$

where S_{Tx} and S_{Rx} are the number of discrete angles at the Tx and Rx, respectively, within the prior ranges. Also for notation brevity, define

$$\begin{aligned} \mathbf{a}_{\text{Tx}}^i &\triangleq \mathbf{a}_{\text{Tx}}(\vartheta^i) & \dot{\mathbf{a}}_{\text{Tx}}^i &\triangleq \dot{\mathbf{a}}_{\text{Tx}}(\vartheta^i) \\ \mathbf{a}_{\text{Rx}}^q &\triangleq \mathbf{a}_{\text{Rx}}(\varphi^q) & \dot{\mathbf{a}}_{\text{Rx}}^q &\triangleq \dot{\mathbf{a}}_{\text{Rx}}(\varphi^q). \end{aligned} \quad (22)$$

Then, by replacing the continuous set by the grid, and since the DEB/OEB formulas (5)–(6) decouple into a part that depends only on θ and another on ϕ , the left side of (19b)–(19c) can be expressed as

$$\begin{aligned} \min_{(\theta, \phi) \in \mathcal{R}_{\text{Tx}} \times \mathcal{R}_{\text{Rx}}} \text{DEB}^{-1} &= 2 \text{SNR} K_{\text{D}} \\ \min_i \left(\|\mathbf{F}^{\text{H}} \dot{\mathbf{a}}_{\text{Tx}}^i\|_2^2 - \frac{|\mathbf{a}_{\text{Tx}}^{i\text{H}} \mathbf{F} \mathbf{F}^{\text{H}} \dot{\mathbf{a}}_{\text{Tx}}^i|^2}{\|\mathbf{F}^{\text{H}} \mathbf{a}_{\text{Tx}}^i\|_2^2} \right) & \quad (23) \end{aligned}$$

$$\min_{(\theta, \phi) \in \mathcal{R}_{\text{Tx}} \times \mathcal{R}_{\text{Rx}}} \text{OEB}^{-1} = 2 \text{SNR} K_{\text{O}} \min_i \|\mathbf{F}^{\text{H}} \mathbf{a}_{\text{Tx}}^i\|_2^2 \quad (24)$$

where K_{D} and K_{O} are the following constants (they do not depend on the optimizing variables \mathbf{F} or t)

$$K_{\text{D}} \triangleq \min_q \|\mathbf{W}^{\text{H}} \mathbf{a}_{\text{Rx}}^q\|_2^2 \quad (25)$$

$$K_{\text{O}} \triangleq \min_q \left(\|\mathbf{W}^{\text{H}} \dot{\mathbf{a}}_{\text{Rx}}^q\|_2^2 - \frac{|\mathbf{a}_{\text{Rx}}^{q\text{H}} \mathbf{W} \mathbf{W}^{\text{H}} \dot{\mathbf{a}}_{\text{Rx}}^q|^2}{\|\mathbf{W}^{\text{H}} \mathbf{a}_{\text{Rx}}^q\|_2^2} \right). \quad (26)$$

Combining (19) with (23)–(24), results in

$$\max_{\mathbf{F}, t} t \quad (27a)$$

$$\text{s.t.} \quad K_{\text{D}} \left(\|\mathbf{F}^{\text{H}} \dot{\mathbf{a}}_{\text{Tx}}^i\|_2^2 - \frac{|\mathbf{a}_{\text{Tx}}^{i\text{H}} \mathbf{F} \mathbf{F}^{\text{H}} \dot{\mathbf{a}}_{\text{Tx}}^i|^2}{\|\mathbf{F}^{\text{H}} \mathbf{a}_{\text{Tx}}^i\|_2^2} \right) \geq t \quad (27b)$$

$$K_{\text{O}} \|\mathbf{F}^{\text{H}} \mathbf{a}_{\text{Tx}}^i\|_2^2 \geq t \quad (27c)$$

$$\|\mathbf{f}_m\|_2 = 1 \quad m = 1, \dots, M. \quad (27d)$$

for $i = 1, \dots, S_{\text{Tx}}$.

Relaxation on the Energy Constraint: In order to transform (27) into a convex problem, we propose a relaxation of the feasible set. If the solution to the newly relaxed problem is still within the original feasible set, then it is the optimum solution of the original problem. The first proposed relaxation consists on replacing $\|\mathbf{f}_m\|_2 = 1$ for $m = 1, \dots, M$, by $\sum_{m=1}^M \|\mathbf{f}_m\|_2^2 = M$. By taking into account that \mathbf{f}_m is the m -th column of \mathbf{F} and that $\|\mathbf{F}\|_{\text{F}}^2 = \text{Tr} \mathbf{F} \mathbf{F}^{\text{H}}$, the new relaxed constraint can be expressed as $\text{Tr} \mathbf{F} \mathbf{F}^{\text{H}} = M$.

Variable Change: Next, we introduce the following variable change

$$\mathbf{X} = \mathbf{F} \mathbf{F}^{\text{H}}, \quad \text{rank} \mathbf{X} \leq M, \quad \mathbf{X} \succcurlyeq 0, \quad (28)$$

where ‘ $\succcurlyeq 0$ ’ denotes positive semidefinite matrix. The variable change is reversible because \mathbf{F} can always be retrieved from \mathbf{X} by, for instance, a Cholesky decomposition.

Rank Relaxation: The second and final relaxation consists in dropping the rank constraint. Thus, the new optimization problem after including the two relaxations and performing the variable change is

$$\max_{\mathbf{X}, t} t \quad (29a)$$

$$\text{s.t.} \quad K_{\text{D}} \left(\dot{\mathbf{a}}_{\text{Tx}}^{i\text{H}} \mathbf{X} \dot{\mathbf{a}}_{\text{Tx}}^i - \frac{|\mathbf{a}_{\text{Tx}}^{i\text{H}} \mathbf{X} \dot{\mathbf{a}}_{\text{Tx}}^i|^2}{\mathbf{a}_{\text{Tx}}^{i\text{H}} \mathbf{X} \mathbf{a}_{\text{Tx}}^i} \right) \geq t \quad (29b)$$

$$K_{\text{O}} \mathbf{a}_{\text{Tx}}^{i\text{H}} \mathbf{X} \mathbf{a}_{\text{Tx}}^i \geq t \quad (29c)$$

$$\text{Tr} \mathbf{X} = M \quad (29d)$$

$$\mathbf{X} \succcurlyeq 0 \quad (29e)$$

for $i = 1, \dots, S_{\text{Tx}}$. Constraint (29b) can be cast as a second order cone (30b) [31, Chapter 2.3],

$$\max_{\mathbf{X}, t} t \quad (30a)$$

$$\begin{aligned} \left\| \left(\dot{\mathbf{a}}_{\text{Tx}}^{i\text{H}} \mathbf{X} \dot{\mathbf{a}}_{\text{Tx}}^i - \frac{2\mathbf{a}_{\text{Tx}}^{i\text{H}} \mathbf{X} \dot{\mathbf{a}}_{\text{Tx}}^i}{K_{\text{D}}} - \mathbf{a}_{\text{Tx}}^{i\text{H}} \mathbf{X} \mathbf{a}_{\text{Tx}}^i \right) \right\|_2 \\ \leq \dot{\mathbf{a}}_{\text{Tx}}^{i\text{H}} \mathbf{X} \dot{\mathbf{a}}_{\text{Tx}}^i - \frac{t}{K_{\text{D}}} + \mathbf{a}_{\text{Tx}}^{i\text{H}} \mathbf{X} \mathbf{a}_{\text{Tx}}^i \end{aligned} \quad (30b)$$

$$K_{\text{O}} \mathbf{a}_{\text{Tx}}^{i\text{H}} \mathbf{X} \mathbf{a}_{\text{Tx}}^i \geq t \quad (30c)$$

$$\text{Tr} \mathbf{X} = M \quad (30d)$$

$$\mathbf{X} \succcurlyeq 0, \quad (30e)$$

where $i = 1, \dots, S_{\text{Tx}}$. Problem (30) is a conic program [32], and consequently convex, because it is composed of linear constraints, second order cones (30b) and a positive semidefinite cone (30e). An advantage of having reformulated our problem as a conic program is that they are well studied in the literature and very efficient solvers exist [33], [34].

For the solution to Problem 2 simply solve the same problem (30) without constraint (30c). By deleting (30c) and performing the variable change $\frac{t}{K_{\text{D}}} \leftarrow t$, constants K_{O} and K_{D} disappear, making the optimization problem independent of the receiver’s array response. To obtain the solution to Problem 3 delete (30b), and following the same reasoning, the optimization problem also becomes independent of the receiver’s array response.

Remark: When the Tx (or the Rx) is equipped with a uniform linear array (ULA) [35], the DEB (or OEB) tends to infinite at the endfire. This is because, for the ULA case, there exists no unbiased AoD (or AoA) estimator when the endfire is part of the search space. For an in-depth explanation of this phenomenon see [36]. However, as done in many works [37], this problem can be circumvented if one defines a new parameter ‘spatial frequency’ $\omega = \frac{\cos(\theta)}{2}$ (or $\omega = \frac{\cos(\phi)}{2}$) assuming the ULA is aligned along the x -axis, and treats ω as the unknown parameter instead of θ (or ϕ).

D. Recovery of the Precoders

In the previous section, Problem 1 was transformed into a convex problem (30) by

- A) approximating the prior ranges with a grid (20), (21),
- B) relaxing the feasible set by replacing $\|\mathbf{f}_m\|_2 = 1$ for $m = 1, \dots, M$, by $\sum_{m=1}^M \|\mathbf{f}_m\|_2^2 = M$.
- C) change of variables $\mathbf{X} = \mathbf{F}\mathbf{F}^H$, $\text{rank } \mathbf{X} \leq M$, $\mathbf{X} \succeq 0$,
- D) relaxing the feasible set by dropping $\text{rank } \mathbf{X} \leq M$.

We abuse the notation and call \mathbf{X} the global optimum of (30) instead of the optimizing variable. It turns out that the grid approximation (A) is very accurate when made dense enough. Moreover, the trace constraint in (30d) induces a low-rank solution [38], [39]. Hence, if the number of precoders M is sufficiently large, then it will occur that $\text{rank } \mathbf{X} \leq M$, and the relaxation (D) will not affect the solution. Thus, in the remainder of this section we discuss the effect of (B) and (C) assuming A and D are exact. These two later assumptions will be validated numerically in Section IV-A.

Given \mathbf{X} , the variable change (C) can be reversed by performing a Cholesky decomposition [40]. However, we are interested in a decomposition from \mathbf{X} to \mathbf{F} that also satisfies $\|\mathbf{f}_m\|_2 = 1$ for $m = 1, \dots, M$ (B). If such decomposition existed, then \mathbf{F} could be recovered from \mathbf{X} and satisfy all the constraints to the original Problem 1 in its hypograph form (19). In summary, we need to find \mathbf{F} such that

- C1) $\mathbf{F}\mathbf{F}^H = \mathbf{X}$
- C2) $\text{diag}(\mathbf{F}^H\mathbf{F}) = \mathbf{1}$

where $\text{diag}(\mathbf{F}^H\mathbf{F})$ denotes a vertical vector stacking the entries on the main diagonal of $\mathbf{F}^H\mathbf{F}$. Define $R \triangleq \text{rank } \mathbf{X}$ which by assumption $R \leq M$. It follows from C1 that $\text{rank } \mathbf{F} = R$. Sufficient conditions for satisfying C1 and C2 can be obtained by expanding \mathbf{F} and \mathbf{X} by their *compact* singular value decomposition (SVD) and eigendecomposition (ED), respectively,

$$\mathbf{F} = \mathbf{U}\mathbf{\Sigma}\mathbf{V}^H \quad (31)$$

$$\mathbf{X} = \mathbf{Q}\mathbf{\Lambda}\mathbf{Q}^H, \quad (32)$$

where $\mathbf{U} = [\mathbf{u}_1 \cdots \mathbf{u}_R] \in \mathbb{C}^{N_{\text{Tx}} \times R}$ is a matrix of left singular vectors, $\mathbf{V} = [\mathbf{v}_1 \cdots \mathbf{v}_R] \in \mathbb{C}^{R \times R}$ is a matrix of right singular vectors, $\mathbf{Q} = [\mathbf{q}_1 \cdots \mathbf{q}_R] \in \mathbb{C}^{N_{\text{Tx}} \times R}$ is a matrix of eigenvectors, and $\mathbf{\Sigma}$ and $\mathbf{\Lambda}$ are diagonal matrices whose diagonal elements are the singular values $\mu_1 \cdots \mu_R$ and the eigenvalues $\lambda_1 \cdots \lambda_R$, respectively.

Substituting \mathbf{F} and \mathbf{X} in C1 with (31) and (32), respectively, leads to a new form of C1, $\mathbf{U}\mathbf{\Sigma}^2\mathbf{U}^H = \mathbf{Q}\mathbf{\Lambda}\mathbf{Q}^H$. This equality

can be viewed as a problem of matching the eigenvectors and eigenvalues on both sides of the equation, i.e.,

$$\mathbf{u}_m = \mathbf{q}_m \quad (33)$$

$$\mu_m = \sqrt{\lambda_m}, \quad (34)$$

for $m = 1, \dots, R$. Similarly, substituting (31) and (32) into C2 yields the new condition

$$\text{diag}(\mathbf{V}\mathbf{\Sigma}^2\mathbf{V}^H) = \mathbf{1}. \quad (35)$$

The (diagonal) elements of $\mathbf{\Sigma}$ have been fixed by (34), hence, only \mathbf{V} can be adjusted to meet the new condition. Notice that $\mathbf{Z} \triangleq \mathbf{V}\mathbf{\Sigma}^2\mathbf{V}^H$ may be regarded as the eigendecomposition of a matrix whose non-zero eigenvalues are $\mu_1^2 \dots, \mu_R^2$ and their corresponding eigenvectors $\mathbf{v}_1, \dots, \mathbf{v}_R$. Consequently, condition (35) is equivalent to the existence of a matrix \mathbf{Z} with prescribed non-zero eigenvalues $\mu_1^2 \dots, \mu_R^2$ and main diagonal filled with 1’s. Fortunately, for the particular case of constant diagonal, the Schur-Horn theorem [41, B.1. in p. 218] states that \mathbf{Z} always exists, and it can be obtained by the Bendel-Mickey algorithm [42], [43].

Remark: The solution to (35) is in general not unique, and so the Bendel-Mickey algorithm is designed to return a random solution in the solution set. Consequently, the solution to Problems 1 to 3 is random as well.

In summary, the different pieces of a valid \mathbf{F} satisfying C1 and C2 can be obtained as follows: its left singular vectors by (33), its singular values by (34) and its right singular vectors by finding a matrix satisfying (35) with the Bendel-Mickey algorithm and computing its eigenvectors. All these steps are summarized in Algorithm 1.

Algorithm 1 Retrieval of the optimal precoders \mathbf{F} from \mathbf{X}

inputs: \mathbf{X}, M

outputs: \mathbf{F}

- 1: compute the *compact* ED of $\mathbf{X} = \mathbf{Q}\mathbf{\Lambda}\mathbf{Q}^H$ where the diagonal elements of $\mathbf{\Lambda}$ are $\lambda_1, \dots, \lambda_R$ and $R = \text{rank } \mathbf{X}$
 - 2: find a matrix \mathbf{Z} with eigenvalues $\lambda_1, \dots, \lambda_R$ and all diagonal elements 1 with the Bendel-Mickey algorithm³ [42], [43]
 - 3: compute the ED of \mathbf{Z} and denote $\mathbf{v}_1, \dots, \mathbf{v}_R$ the eigenvectors associated to eigenvalues $\lambda_1, \dots, \lambda_R$
 - 4: set $\mathbf{F} = \mathbf{Q}\mathbf{\Lambda}^{\frac{1}{2}}[\mathbf{v}_1 \cdots \mathbf{v}_R]^H$
-

Examples: Fig. 1 plots the beampatterns (gain vs. azimuth) of the AoD-AoA-optimal precoders. The gain and aggregated gain⁴ are defined in (8) and (9), respectively. The yellow zone in the figures represents the prior range on the AoD. Furthermore, we define the term ‘worst aggregated gain’, as the lowest aggregated gain within the prior range. As expected from the interpretation in Section III, where it was argued that the OEB is optimized when the gain $\|\mathbf{F}^H\mathbf{a}_{\text{Tx}}(\theta)\|_2$ is maximized, in Fig. 1c the AoA-optimal precoders’ worst aggregated gain is 14.1 dB, which is the highest among the three subfigures. The AoD-optimal precoders in

³Code available in Matlab R2015b by the name `gallery('randcorr', arg)`.

⁴To convert the (aggregated) gain to dB we apply the function $20 \log_{10}(\cdot)$.

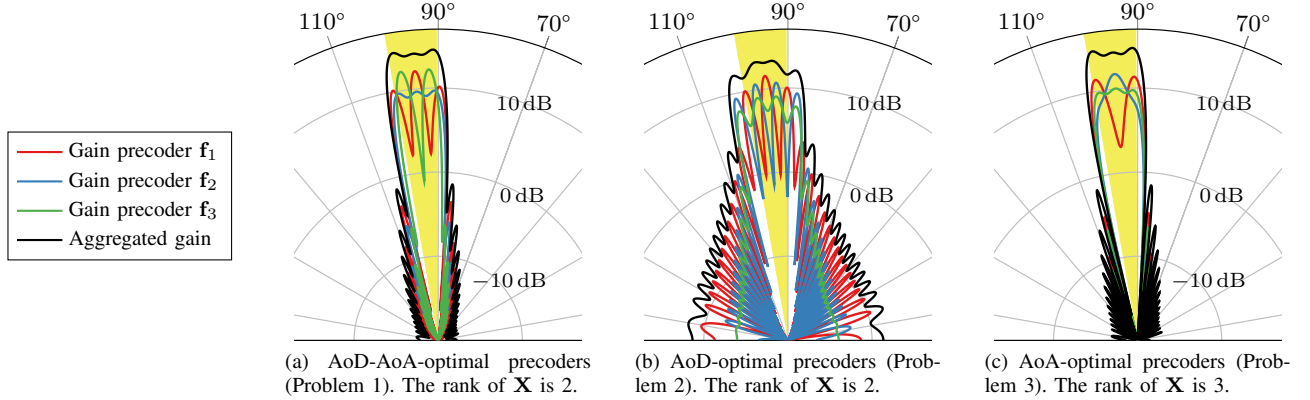


Fig. 1. Array gain of the precoders vs. azimuth for all M precoders. The Tx and Rx are equipped with 30-antenna half-wavelength inter antenna spacing uniform linear array (ULA) [35]. The number of training sequences is $M = 3$. The AoD (same for the AoA for simplicity) is known a priori to lie in the range $[90^\circ, 100^\circ]$, indicated by the yellow shaded area. According to Section III-D, the optimality of these precoders is ensured because for all cases $M \geq \text{rank } \mathbf{X}$.

Fig. 1b show a large number of ripples, which is also consistent with the interpretation in Section III. The intuitive explanation is that the Rx identifies the AoD by observing the changes of received signal strength and phase changes for the M training sequences. Thus, in order to increase the AoD estimation accuracy, the Tx's precoders gain and phase for closely spaced AoD must be as different as possible. The AoD-optimal precoders worst aggregated gain, 13.6 dB, is just slightly worse than that of the AoA-optimal precoders. Lastly, the AoD-AoA-optimal precoders offer a trade-off between the AoA-optimal and AoD-optimal precoders in terms of aggregated gain and 'ripples'.

Interestingly, in most of the literature, the traditional approach to AoD (and AoA) estimation is to split the prior range into multiple disjoint subranges, and design precoders that have a high flat gain in the subrange and low gain for the rest of directions [8], [22], [44], hence the term "sector beams" among others. However, if the sector beams were to achieve an ideal beampattern, i.e., $\mathbf{f}_m^H \mathbf{a}_{\text{Tx}}(\theta) = g_{\text{max}}$ for θ inside the subrange, and $\mathbf{f}_m^H \mathbf{a}_{\text{Tx}}(\theta) = 0$ elsewhere; then, the DEB (5) would be infinite because $\frac{d}{d\theta} \mathbf{F}^H \mathbf{a}_{\text{Tx}}(\theta) = 0$. Conceptually, ideal sector beams are bad for precise AoD estimation because perturbations of the AoD within a subrange do not change the received signal.

E. Additional Constraints

The proposed precoders are purely oriented to minimizing the CRB of the AoD and/or AoA. However, in practice some additional constraints may be desired, such as null steering towards certain directions in order to mitigate multi user interference or cancel certain paths. Next, it is shown how some of these constraints can easily be added to the original optimization problems.

1) *Identifiability of the AoD and AoA*: A necessary condition for correctly estimating the AoD and/or AoA is that they are identifiable. Otherwise, even in the absence of noise, we may suffer from large estimation errors due to signal ambiguities. This may sound counterintuitive, since Problems 1–3 minimized the CRB on the AoD/AoA which is a tight lower-bound on the estimators variance. However, the caveat here is

that the CRB is tight only when the estimation errors are small, or in plain words, the CRB only takes care of the errors in the vicinity of the true AoD and dismisses large errors due to signal ambiguities. By imposing an identifiability constraint, we can observe in Section IV-B that the SNR region over which the CRB is tight is enlarged. The AoA and AoD are identifiable provided that the received signals (4) in absence of noise are different

$$\alpha \mathbf{W}^H \mathbf{a}_{\text{Rx}}(\phi) \mathbf{a}_{\text{Tx}}^H(\theta) \mathbf{F} \neq \alpha' \mathbf{W}^H \mathbf{a}_{\text{Rx}}(\phi') \mathbf{a}_{\text{Tx}}^H(\theta') \mathbf{F}, \quad (36)$$

for all possible $\theta \neq \theta'$ in \mathcal{R}_{Tx} , $\phi \neq \phi'$ in \mathcal{R}_{Rx} , or $\alpha \neq \alpha'$. Since the signals are rank 1 matrices, the condition decouples into pair-wise linear independence between steering vectors at the Rx and Tx:

$$\beta \mathbf{W}^H \mathbf{a}_{\text{Rx}}(\phi) \neq \beta' \mathbf{W}^H \mathbf{a}_{\text{Rx}}(\phi') \quad (37)$$

$$\gamma \mathbf{F}^H \mathbf{a}_{\text{Tx}}(\theta) \neq \gamma' \mathbf{F}^H \mathbf{a}_{\text{Tx}}(\theta') \quad (38)$$

for all complex $\beta, \beta', \gamma, \gamma'$ different than zero. Condition (37) depends on the Rx array response and the combiner \mathbf{W} . For the particular case of a fully digital Rx ($\mathbf{W} = \mathbf{I}$), this condition is in general satisfied for most common types of arrays [45], [46]. Our focus is in the design of the precoders, thus we turn to condition (38). This condition depends on the Tx array response and on the precoders \mathbf{F} . Thus, careful attention needs to be put on the precoders to avoid creating ambiguities.

Pair-wise linear independence (38) is equivalent to $|\mathbf{a}_{\text{Tx}}^H(\theta) \mathbf{F}^H \mathbf{F}^H \mathbf{a}_{\text{Tx}}(\theta')|^2 \|\mathbf{F}^H \mathbf{a}_{\text{Tx}}(\theta)\|_2^{-2} \|\mathbf{F}^H \mathbf{a}_{\text{Tx}}(\theta')\|_2^{-2} < 1$. Thus, in order to ensure that the AoD is identifiable we propose to add the following constraints to problem (30):

$$\frac{|\mathbf{a}_{\text{Tx}}^H(\vartheta^i) \mathbf{F}^H \mathbf{F}^H \mathbf{a}_{\text{Tx}}(\vartheta^{i'})|^2}{\|\mathbf{F}^H \mathbf{a}_{\text{Tx}}(\vartheta^i)\|_2^2 \|\mathbf{F}^H \mathbf{a}_{\text{Tx}}(\vartheta^{i'})\|_2^2} < \rho \quad (39)$$

for all i, i' such that $\vartheta^i - \vartheta^{i'} > D(\text{mod } 2\pi)$, where

$0 \leq \rho < 1$ and D is the angular resolution of the array⁵. By performing the variable change $\mathbf{X} = \mathbf{F}\mathbf{F}^H$ and some algebraic manipulations [31], (39) can be expressed as a second order cone (convex constraint):

$$\left\| \begin{pmatrix} 2 \mathbf{a}_{\text{Tx}}^{iH} \mathbf{X} \mathbf{a}_{\text{Tx}}^{i'} \\ \sqrt{\rho} \mathbf{a}_{\text{Tx}}^{iH} \mathbf{X} \mathbf{a}_{\text{Tx}}^i - \sqrt{\rho} \mathbf{a}_{\text{Tx}}^{i'H} \mathbf{X} \mathbf{a}_{\text{Tx}}^{i'} \end{pmatrix} \right\|_2 \leq \sqrt{\rho} \mathbf{a}_{\text{Tx}}^{iH} \mathbf{X} \mathbf{a}_{\text{Tx}}^i + \sqrt{\rho} \mathbf{a}_{\text{Tx}}^{i'H} \mathbf{X} \mathbf{a}_{\text{Tx}}^{i'}, \quad (40)$$

where the shortened notation (22) was used. This condition must be added to optimization problem (30) whenever we wish to estimate the AoD because it ensures it is identifiable.

2) *Out-of-Range Attenuation*: From Fig. 1, we can observe that the precoders radiate some non-negligible energy in other directions out of the prior range \mathcal{R}_{Tx} . In practice there may be some operational constraints such as low sidelobe ratio [47] for improved inter-user interference or the placement of nulls in certain areas of the beampattern. Let $\{\pi^q\}_{q=1}^{S_a}$ be the AoDs for which we wish to enforce a lower transmitting power, and recall $\{\vartheta^i\}_{i=1}^{S_{\text{Tx}}}$ is the grid of angles within the prior range (20). The total transmitted energy in direction π^q over the M training sequences is $\|\mathbf{F}^H \mathbf{a}_{\text{Tx}}(\pi^q)\|_2^2$. Let $A_q < 1$ be the desired attenuation factor, then, we propose to add the following constraint to problem (30),

$$\|\mathbf{F}^H \mathbf{a}_{\text{Tx}}(\pi^q)\|_2^2 \leq A_q \|\mathbf{F}^H \mathbf{a}_{\text{Tx}}(\vartheta^i)\|_2^2 \quad (41)$$

for $q = 1, \dots, S_a$ and $i = 1, \dots, S_{\text{Tx}}$, which can be transformed to linear constraints after performing the variable change $\mathbf{X} = \mathbf{F}\mathbf{F}^H$,

$$\mathbf{a}_{\text{Tx}}^H(\pi^q) \mathbf{X} \mathbf{a}_{\text{Tx}}(\pi^q) \leq A_q \mathbf{a}_{\text{Tx}}^H(\vartheta^i) \mathbf{X} \mathbf{a}_{\text{Tx}}(\vartheta^i). \quad (42)$$

These $S_a S_{\text{Tx}}$ constraints can be reduced to $S_a + S_{\text{Tx}}$ by incorporating a dummy variable z ,

$$\mathbf{a}_{\text{Tx}}^H(\pi^q) \mathbf{X} \mathbf{a}_{\text{Tx}}(\pi^q) \leq A_q z \quad q = 1, \dots, S_a \quad (43)$$

$$\mathbf{a}_{\text{Tx}}^H(\vartheta^i) \mathbf{X} \mathbf{a}_{\text{Tx}}(\vartheta^i) \geq z \quad i = 1, \dots, S_{\text{Tx}}. \quad (44)$$

Examples: Fig. 2 plots the left hand side of (39) when the precoders are obtained with or without the identifiability constraint. Ideally, only the anti-diagonal across the white square should be red as is the case in the right figure. The left figure, has two red stripes, and therefore, there are pairs of AoDs within the range \mathcal{R}_{Tx} which result in the same signals, and consequently are not identifiable even in the absence of noise.

In Fig. 3 two sets of AoD-AoA-optimal precoders are generated. The first set of precoders has no constraint on the aggregated gain (9) towards directions outside of the range of interest \mathcal{R}_{Tx} . The second set of precoders imposes a 20 dB attenuation in the range $[150^\circ, 220^\circ]$ and a null at 310° . Note that the aggregated gain within the range is virtually the same for both sets of precoders.

⁵The resolution of the array is typically related to the antenna aperture and is different for each array configuration. In practice, one could start with an approximate value and then tweak this parameter. For instance, for an N -antennas half-wavelength inter-antenna spaced uniform circular array (UCA) [35], the angle resolution has been checked numerically to be well approximately by $1.6 \sin(\pi/N)$ [radians].

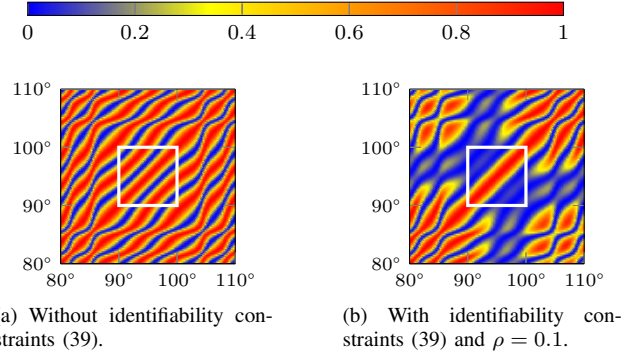


Fig. 2. Colormap of left hand side of (39) versus θ and θ' when employing AoD-AoA-optimal beams. The Tx and the Rx have, each, a 30-antennas UCA. The number of training sequences $M = 4$ and the rank of \mathbf{X} is 4. It is known a priori that the AoD lies in the interval $\mathcal{R}_{\text{Tx}} = [90^\circ, 100^\circ]$. The white square indicates the region $\mathcal{R}_{\text{Tx}} \times \mathcal{R}_{\text{Tx}}$.

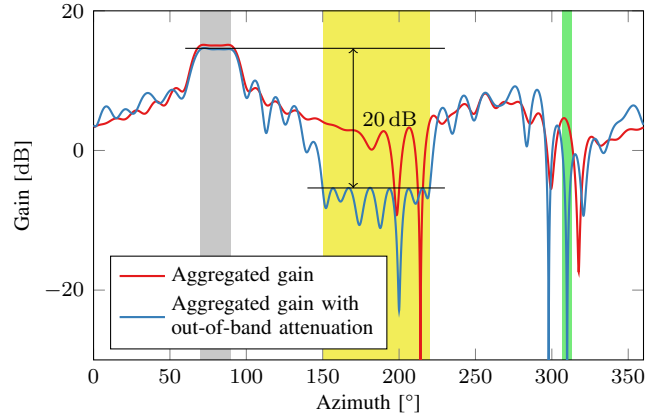


Fig. 3. Aggregated gain (9) of the AoD-AoA-optimal precoders vs. azimuth. The Tx and Rx are equipped with 30-antenna half-wavelength inter antenna spacing UCA. The number of training sequences is $M = 3$ and the rank \mathbf{X} is 2, ensuring the precoders are optimal. The AoD (same for the AoA for simplicity) is known a priori to lie in the range $[70^\circ, 90^\circ]$, indicated by the grey shaded bin. Two different sets of precoders are used. First set is the optimum solution to Problem 1. The second set is the optimum solution to Problem 1 while imposing a 20 dB attenuation in the range $[150^\circ, 220^\circ]$ indicated by the yellow shaded bin, and a null at 310° indicated by the green shaded bin.

IV. NUMERICAL RESULTS

The performance of the optimal precoders is illustrated by multiple Monte Carlo simulations. To this end, we define the following figures of merit which are in fact the square roots of the objective functions of Problems 1–3, respectively,

$$\text{Worst case rEB} = \sqrt{\max_{(\theta, \phi) \in \mathcal{R}_{\text{Tx}} \times \mathcal{R}_{\text{Rx}}} \text{EB}} \quad (45)$$

$$\text{Worst case rDEB} = \sqrt{\max_{(\theta, \phi) \in \mathcal{R}_{\text{Tx}} \times \mathcal{R}_{\text{Rx}}} \text{DEB}} \quad (46)$$

$$\text{Worst case rOEB} = \sqrt{\max_{(\theta, \phi) \in \mathcal{R}_{\text{Tx}} \times \mathcal{R}_{\text{Rx}}} \text{OEB}}, \quad (47)$$

where $\text{EB} = \max\{\text{DEB}, \text{OEB}\}$ and the ‘r’ denotes square root. Sections IV-B–IV-C perform Monte Carlo simulations using 30-antenna uniform circular arrays (UCA) [35] with an inter-antenna spacing of half wavelength. The SNR (7) is fixed

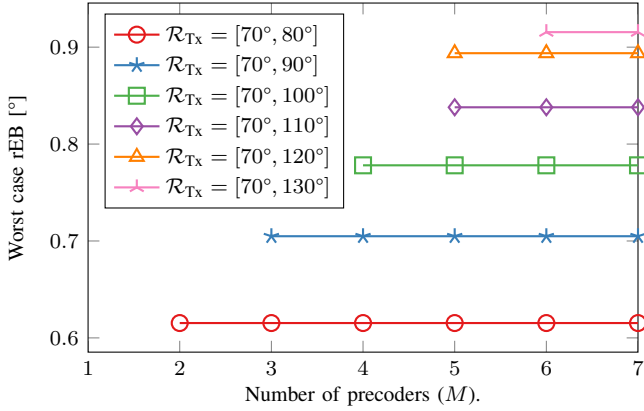


Fig. 4. The total training time is fixed, and consequently the duration of each training sequence decreases inversely proportional to M . Both, the Tx and the Rx, equip a UCA. For simplicity, the prior range on the AoD and AoA are set equal, i.e., $\mathcal{R}_{\text{Rx}} = \mathcal{R}_{\text{Tx}}$.

to -10 dB and the number of transmitted training sequences is $M = 5$. The correlation parameter, defined in Section III-E1, which ensures identifiability of the AoD is set to $\rho = 0.6$ for the AoD- and AoD-AoA-optimal precoders. The prior ranges on the AoD and AoA are, both, $[70^\circ, 90^\circ]$. The Monte Carlo simulations repeat the experiment 100 times, and for each repetition the AoD/AoA are drawn from a uniform random distribution within their prior ranges.

A. Optimality of the Proposed Algorithms

In Section III-D, the solution to Problems 1 to 3 was obtained by approximating the prior ranges on the AoD/AoA with a grid of discrete angles. According to the analysis in Section III-D if the grid approximation is exact and $\text{rank } \mathbf{X} < M$, where \mathbf{X} is the solution to the convex problem (30), then Algorithm 1 can retrieve the optimal precoders \mathbf{F} for Problems 1 to 3. To verify that the grid is a good approximation, we have computed the optimal precoders for the three problems for different grid sizes. Naturally, we expect that denser grids will lead to better approximations. We have found out that the worst case rEB, rDEB and rOEB for the AoD-AoA-, AoD- and AoA-optimal precoders of Problems 1 to 3, respectively, quickly converges to a constant value as the grid becomes denser. In particular, the precoders computed with 8 grid points are less than 0.1% worse than precoders computed with 100 grid points.

Fig. 4 plots the worst case (w.c.) rEB of the optimal AoD-AoA-precoders for varying M while keeping the total training duration constant. Parameter M represents the number of training sequences with different precoding weights. For the cases that $M < \text{rank } \mathbf{X}$, no values of the w.c. rEB are plotted because Algorithm 1 cannot retrieve the optimal precoders \mathbf{F} from \mathbf{X} . It turns out that \mathbf{X} is invariant with M except for a scaling factor (30d). For each prior range \mathcal{R}_{Tx} , the smallest value of M in the curve represents the rank of \mathbf{X} (e.g., $\text{rank } \mathbf{X} = 2$ for $\mathcal{R}_{\text{Tx}} = [70^\circ, 80^\circ]$). For $M \geq \text{rank } \mathbf{X}$, the w.c. rEB remains constant irrespective of M . In other words, a higher transmit diversity M (or number of distinct precoders) does not translate into better estimation

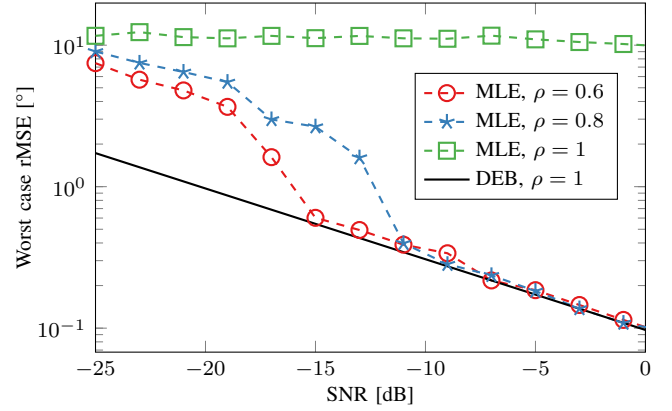


Fig. 5. AoD estimation accuracy vs. SNR for different values of ρ (defined in Section III-E1). Both, the Tx and the Rx, employ UCA. The AoD (same for the AoA for simplicity) is known a priori to lie in the range $[70^\circ, 90^\circ]$.

accuracy if $M \geq \text{rank } \mathbf{X}$. Therefore, $\text{rank } \mathbf{X}$ can be regarded as the minimum transmit diversity necessary for achieving optimal estimation accuracy for a given total training duration. Naturally, the required Tx diversity increases with the size of the range of angles that needs to be covered \mathcal{R}_{Tx} . This observation carries over to the AoD-optimal precoders when analyzed in terms of w.c. rDEB. However, when analyzing the AoA-optimal precoders in terms of w.c. rOEB, the required Tx diversity remains $\text{rank } \mathbf{X} = 2$ for any \mathcal{R}_{Tx} . Our hypothesis is that the required Tx diversity is lower when we do not need to ensure that the AoD is identifiable.

B. Estimators and Ambiguities

Let $\hat{\theta}$ be an estimate on the AoD. Then, the worst case root mean square error on the AoD is defined as

$$\text{Worst case rMSE} = \sqrt{\max_{(\theta, \phi) \in \mathcal{R}_{\text{Tx}} \times \mathcal{R}_{\text{Rx}}} \mathbb{E} \left(\hat{\theta} - \theta \right)^2}. \quad (48)$$

If the MSE is tight to the DEB, such as is the case of the ML estimator, then the w.c. rMSE is tight to the w.c. rDEB. Fig. 5 plots the w.c. rMSE for the MLE (computed by exhaustive search) for different values of ρ . As expected, the MLE's w.c. rMSE converges to the w.c. rDEB for a sufficient large SNR. For decreasing values of ρ , the SNR threshold (which is the SNR value at which the estimators' accuracy matches the lower-bound) is shifted to the left. For $\rho = 1$, the identifiability constraint is removed and the MLE fails to correctly estimate the AoD for any given SNR. Coarsely speaking, ρ controls the degree of maximum *similarity* between the received signals for any two pair of AoD, where $\rho = 0$ imposes signal orthogonality and $\rho = 1$ removes the constraint. Thus, as ρ decreases from 1 to 0, the received signals for any two AoD become less similar and more resilient to noise.

C. Optimal Precoders vs. Sector Beams

Many existing works on codebook design for mmWave channel estimation use the so-called sector beams [6], [16], [23]. In such approaches the regions \mathcal{R}_{Tx} and/or \mathcal{R}_{Rx} are split

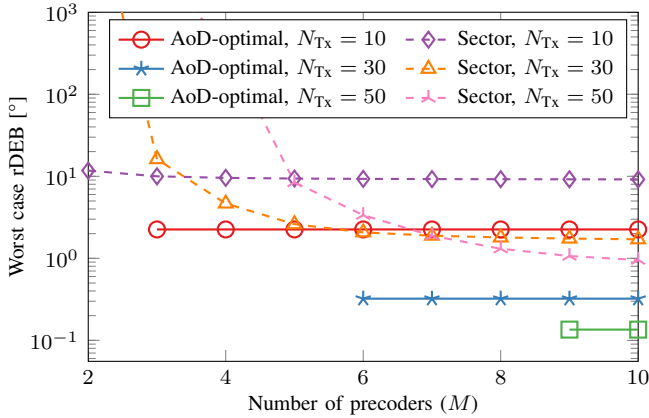


Fig. 6. Performance comparison between AoD-optimal precoders and sector beams. Both, the Tx and the Rx, equip a ULA. The AoD (same for the AoA for simplicity) is known a priori to lie in the range $[70^\circ, 90^\circ]$.

evenly into M subregions. Ideally, each beam has maximum gain in one of these disjoint subregions and zero gain anywhere else. Then, the channel is sounded sequentially in time with all possible pairs of precoders and combiners. By detecting the pair leading to the largest power at the receiver, one can estimate the AoD and/or AoA with beamwidth accuracy. Its widespread use is due to the simplicity of the approach, despite not necessary being optimal in the sense of minimizing the mean error. Moreover, only approximate sector beams can be generated in practice because of the sharp discontinuities in the beampattern.

Since this work does not deal with the design of optimal combiners, we compare the proposed optimal precoders with a set of sector beams at the Tx only, and assume a fully digital array at the Rx, i.e., $\mathbf{W} = \mathbf{I}$. To design the sector beams we use classical tools from filter design [48, Chapter 1.5.1]. Fig 6 plots the w.c. rDEB for AoD-optimal precoders and sector beams. As outlined in Section IV-A, the accuracy of the AoD-optimal precoders remains constant for any M larger than rank \mathbf{X} . The AoD-optimal precoders outperform the sector beams by an order of magnitudes. An interesting phenomenon is that as the number of antennas increases, the sector beams become tend to the ideal sector shape with a flat top and low gain outside the main lobe. However, while such beams are ideal for beam pairing, they lead to poor AoD estimation accuracy due to the fact that the received signals are similar for closely spaced AoDs.

D. AoA Versus AoD Estimation

To estimate the AoA, it is necessary that the Rx equips an array of antennas, whereas for AoD estimation, the Tx must equip the array. It is a common misconception that, assuming the same exact array in Tx or Rx mode, AoA estimation is better than AoD estimation in terms of accuracy. For instance, in [30] the authors argue that if a base station has an array with many antennas, then in order to find the direction of the user, it is more accurate to perform uplink AoA estimation instead of downlink AoD estimation. However, as we show next such difference in performance is not a fundamental limit but rather

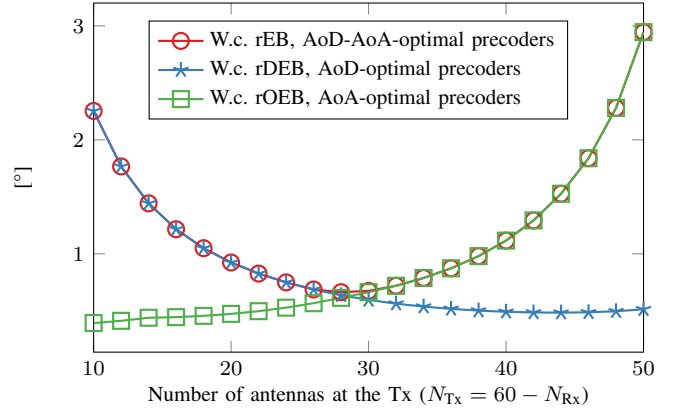


Fig. 7. Comparison between AoD and AoA estimation. The total number of antennas at the Tx and Rx are kept constant to 60 antennas; so as the number of Tx antennas increases, the number of Rx antennas decreases, and vice-versa. The AoD and AoA are known a priori to lie in the range $[70^\circ, 90^\circ]$.

a result of not optimizing the precoders. Fig. 7 plots metrics (45)–(47) for the optimal precoders when the total number of antennas at the Tx and Rx is fixed to 60. The goal of this experiment is to observe the effect of different array sizes at the Tx and Rx in the estimation accuracy of the AoD and AoA. The left side of the plot represents the case where the Tx has only 10 antennas and the Rx has 50 antennas. Consequently, the AoA estimation accuracy is best. On the contrary, on the right side of the plot, the Tx array is larger than the Rx array, and so the AoD estimation accuracy. If the goal was to estimate the direction of a path, notice that the best accuracy achieved in AoA or AoD is approximately the same $\sim 0.4^\circ$.

V. CONCLUSIONS

This paper dealt with the design of precoders for mmWave communication, optimized for estimating the AoD and AoA under a given uncertainty range. Our focus was on a single propagation path, assuming that such a path has been identified for precoding and combining so that weaker paths can be ignored. The design is based on minimizing the worst-case CRB of the AoD and AoA, which is a tight lower-bound to the variance of MLE at medium-to-high SNRs. Through a convex reformulation, optimal precoders are recovered, which turn out to have different properties than traditional sector beams and perform an order of magnitude better. We found that beyond a certain number of precoders at the Tx, the CRB on the AoD/AoA does not improve and that the minimum number of precoders for optimal performance is a side-product of the optimization procedure. Finally, numerical evidence shows an array can estimate the direction of a path in transmit (AoD) or receive (AoA) mode with equal accuracy when using the optimal precoders.

APPENDIX

Assume perfect time synchronization, then the log-likelihood function of the observations (4) after neglecting constant terms is proportional to

$$\log \rho(\mathbf{Y}|\theta, \phi, \alpha) \propto -\frac{1}{\sigma^2} \|\mathbf{Y} - \|\mathbf{s}\|_2 \mathbf{W}^H \mathbf{H} \mathbf{F}\|_F^2, \quad (49)$$

where \mathbf{H} , defined in (2), depends on the unknown parameters. According to the analysis of [24], the Fisher information matrix of the unknown parameters turns out to be

$$\mathbf{J} = \begin{bmatrix} \Phi_{\theta,\theta} & \Phi_{\theta,\phi} & \Phi_{\theta,\Re\alpha} & \Phi_{\theta,\Im\alpha} \\ \Phi_{\theta,\phi} & \Phi_{\phi,\phi} & \Phi_{\phi,\Re\alpha} & \Phi_{\phi,\Im\alpha} \\ \Phi_{\theta,\Re\alpha} & \Phi_{\phi,\Re\alpha} & \Phi_{\Re\alpha,\Re\alpha} & 0 \\ \Phi_{\theta,\Im\alpha} & \Phi_{\phi,\Im\alpha} & 0 & \Phi_{\Im\alpha,\Im\alpha} \end{bmatrix}, \quad (50)$$

where⁶

$$\Phi_{\theta,\theta} = 2 \text{SNR} \|\tilde{\mathbf{a}}_{\text{Rx}}(\phi)\|_2^2 \|\dot{\tilde{\mathbf{a}}}_{\text{Tx}}(\theta)\|_2^2 \quad (51a)$$

$$\Phi_{\phi,\phi} = 2 \text{SNR} \|\dot{\tilde{\mathbf{a}}}_{\text{Rx}}(\phi)\|_2^2 \|\tilde{\mathbf{a}}_{\text{Tx}}(\theta)\|_2^2 \quad (51b)$$

$$\Phi_{\Re\alpha,\Re\alpha} = \Phi_{\Im\alpha,\Im\alpha} = \frac{2\|s\|_2^2}{\sigma^2} \|\tilde{\mathbf{a}}_{\text{Rx}}(\phi)\|_2^2 \|\tilde{\mathbf{a}}_{\text{Tx}}(\theta)\|_2^2 \quad (51c)$$

$$\Phi_{\theta,\phi} = 2 \text{SNR} \Re \left[\tilde{\mathbf{a}}_{\text{Rx}}^{\text{H}}(\phi) \dot{\tilde{\mathbf{a}}}_{\text{Rx}}(\phi) \tilde{\mathbf{a}}_{\text{Tx}}^{\text{H}}(\theta) \dot{\tilde{\mathbf{a}}}_{\text{Tx}}(\theta) \right] \quad (51d)$$

$$\Phi_{\theta,\Re\alpha} = \frac{2\|s\|_2^2}{\sigma^2} \|\tilde{\mathbf{a}}_{\text{Rx}}(\phi)\|_2^2 \Re \left[\alpha \dot{\tilde{\mathbf{a}}}_{\text{Tx}}^{\text{H}}(\theta) \tilde{\mathbf{a}}_{\text{Tx}}(\theta) \right] \quad (51e)$$

$$\Phi_{\theta,\Im\alpha} = \frac{2\|s\|_2^2}{\sigma^2} \|\tilde{\mathbf{a}}_{\text{Rx}}(\phi)\|_2^2 \Im \left[\alpha \dot{\tilde{\mathbf{a}}}_{\text{Tx}}^{\text{H}}(\theta) \tilde{\mathbf{a}}_{\text{Tx}}(\theta) \right] \quad (51f)$$

$$\Phi_{\phi,\Re\alpha} = \frac{2\|s\|_2^2}{\sigma^2} \Re \left[\alpha \tilde{\mathbf{a}}_{\text{Rx}}^{\text{H}}(\phi) \dot{\tilde{\mathbf{a}}}_{\text{Rx}}(\phi) \right] \|\tilde{\mathbf{a}}_{\text{Tx}}(\theta)\|_2^2 \quad (51g)$$

$$\Phi_{\phi,\Im\alpha} = \frac{2\|s\|_2^2}{\sigma^2} \Im \left[\alpha \tilde{\mathbf{a}}_{\text{Rx}}^{\text{H}}(\phi) \dot{\tilde{\mathbf{a}}}_{\text{Rx}}(\phi) \right] \|\tilde{\mathbf{a}}_{\text{Tx}}(\theta)\|_2^2, \quad (51h)$$

$\tilde{\mathbf{a}}_{\text{Rx}}(\phi) \triangleq \mathbf{W}^{\text{H}} \mathbf{a}_{\text{Rx}}(\phi)$, $\dot{\tilde{\mathbf{a}}}_{\text{Rx}}(\phi) \triangleq \frac{d}{d\phi} \mathbf{W}^{\text{H}} \mathbf{a}_{\text{Rx}}(\phi)$, $\tilde{\mathbf{a}}_{\text{Tx}}(\theta) \triangleq \mathbf{F}^{\text{H}} \mathbf{a}_{\text{Tx}}(\theta)$, $\dot{\tilde{\mathbf{a}}}_{\text{Tx}}(\theta) \triangleq \frac{d}{d\theta} \mathbf{F}^{\text{H}} \mathbf{a}_{\text{Tx}}(\theta)$ and $\text{SNR} = |\alpha|^2 \|s\|_2^2 \sigma^{-2}$. The CRB requires inverting the FIM. Define

$$\mathbf{J}_{11} = \begin{bmatrix} \Phi_{\theta,\theta} & \Phi_{\theta,\phi} \\ \Phi_{\theta,\phi} & \Phi_{\phi,\phi} \end{bmatrix} \quad (52)$$

$$\mathbf{J}_{12} = \mathbf{J}_{21}^T = \begin{bmatrix} \Phi_{\theta,\Re\alpha} & \Phi_{\theta,\Im\alpha} \\ \Phi_{\phi,\Re\alpha} & \Phi_{\phi,\Im\alpha} \end{bmatrix} \quad (53)$$

$$\mathbf{J}_{22} = \begin{bmatrix} \Phi_{\Re\alpha,\Re\alpha} & 0 \\ 0 & \Phi_{\Im\alpha,\Im\alpha} \end{bmatrix}. \quad (54)$$

Then, by the block matrix inversion formula, the CRB on the AoD and AoA is

$$(\mathbf{J}_{11} - \mathbf{J}_{12} \mathbf{J}_{22}^{-1} \mathbf{J}_{21})^{-1} = \begin{bmatrix} \text{DEB} & 0 \\ 0 & \text{OEB} \end{bmatrix} \quad (55)$$

where

$$\text{DEB}^{-1} = 2 \text{SNR} \|\tilde{\mathbf{a}}_{\text{Rx}}(\phi)\|_2^2 \left(\|\dot{\tilde{\mathbf{a}}}_{\text{Tx}}(\theta)\|_2^2 - \frac{|\tilde{\mathbf{a}}_{\text{Tx}}^{\text{H}}(\theta) \dot{\tilde{\mathbf{a}}}_{\text{Tx}}(\theta)|^2}{\|\tilde{\mathbf{a}}_{\text{Tx}}(\theta)\|_2^2} \right) \quad (56)$$

$$\text{OEB}^{-1} = 2 \text{SNR} \|\tilde{\mathbf{a}}_{\text{Tx}}(\theta)\|_2^2 \left(\|\dot{\tilde{\mathbf{a}}}_{\text{Rx}}(\phi)\|_2^2 - \frac{|\tilde{\mathbf{a}}_{\text{Rx}}^{\text{H}}(\phi) \dot{\tilde{\mathbf{a}}}_{\text{Rx}}(\phi)|^2}{\|\tilde{\mathbf{a}}_{\text{Rx}}(\phi)\|_2^2} \right). \quad (57)$$

REFERENCES

- [1] W. Roh, J.-Y. Seol, J. Park, B. Lee, J. Lee, Y. Kim, J. Cho, K. Cheun, and F. Aryanfar, "Millimeter-wave beamforming as an enabling technology for 5G cellular communications: theoretical feasibility and prototype results," *IEEE Communications Magazine*, vol. 52, no. 2, pp. 106–113, 2014.
- [2] P. Wang, Y. Li, L. Song, and B. Vucetic, "Multi-gigabit millimeter wave wireless communications for 5G: From fixed access to cellular networks," *IEEE Communications Magazine*, vol. 53, no. 1, pp. 168–178, 2015.
- [3] S. Kutty and D. Sen, "Beamforming for millimeter wave communications: An inclusive survey," *IEEE Communications Surveys & Tutorials*, vol. 18, no. 2, pp. 949–973, 2016.
- [4] T. S. Rappaport, G. R. MacCartney, M. K. Samimi, and S. Sun, "Wide-band millimeter-wave propagation measurements and channel models for future wireless communication system design," *IEEE Transactions on Communications*, vol. 63, no. 9, pp. 3029–3056, 2015.
- [5] W. Keusgen, R. J. Weiler, M. Peter, M. Wisotzki, and B. Göktepe, "Propagation measurements and simulations for millimeter-wave mobile access in a busy urban environment," in *39th International Conference on Infrared, Millimeter, and Terahertz waves*. IEEE, 2014, pp. 1–3.
- [6] A. Alkhateeb, O. El Ayach, G. Leus, and R. W. Heath, "Channel estimation and hybrid precoding for millimeter wave cellular systems," *IEEE Journal of Selected Topics in Signal Processing*, vol. 8, no. 5, pp. 831–846, 2014.
- [7] T. E. Bogale, L. B. Le, and X. Wang, "Hybrid analog-digital channel estimation and beamforming: Training-throughput tradeoff," *IEEE Transactions on Communications*, vol. 63, no. 12, pp. 5235–5249, 2015.
- [8] Z. Xiao, T. He, P. Xia, and X.-G. Xia, "Hierarchical codebook design for beamforming training in millimeter-wave communication," *IEEE Transactions on Wireless Communications*, vol. 15, no. 5, pp. 3380–3392, 2016.
- [9] K. Venugopal, A. Alkhateeb, N. G. Prelcic, and R. W. Heath Jr, "Channel estimation for hybrid architecture based wideband millimeter wave systems," *arXiv preprint arXiv:1611.03046*, 2016.
- [10] J. Rodríguez-Fernández, N. González-Prelcic, and R. W. Heath, "Channel estimation in mixed hybrid-low resolution MIMO architectures for mmWave communication," in *Signals, Systems and Computers, 2016 50th Asilomar Conference on*. IEEE, 2016, pp. 768–773.
- [11] V. Va, T. Shimizu, G. Bansal, R. W. Heath Jr et al., "Millimeter wave vehicular communications: A survey," *Foundations and Trends® in Networking*, vol. 10, no. 1, pp. 1–113, 2016.
- [12] J. Choi, V. Va, N. González-Prelcic, R. Daniels, C. R. Bhat, and R. W. Heath Jr, "Millimeter wave vehicular communication to support massive automotive sensing," *IEEE Communications Magazine*, vol. 54, no. 12, pp. 160–167, 2016.
- [13] P. Sanchis, J. Martinez, J. Herrera, V. Polo, J. Corral, and J. Marti, "A novel simultaneous tracking and direction of arrival estimation algorithm for beam-switched base station antennas in millimeter-wave wireless broadband access networks," in *IEEE Antennas and Propagation Society International Symposium*, vol. 1, 2002, pp. 594–597.
- [14] J. Seo, Y. Sung, G. Lee, and D. Kim, "Training beam sequence design for millimeter-wave MIMO systems: A POMDP framework," *submitted for publication*, 2015.
- [15] J. He, T. Kim, H. Ghauch, K. Liu, and G. Wang, "Millimeter wave MIMO channel tracking systems," in *Globecom Workshops*. IEEE, 2014, pp. 416–421.
- [16] M. Kokshoorn, P. Wang, Y. Li, and B. Vucetic, "Fast channel estimation for millimeter wave wireless systems using overlapped beam patterns," in *IEEE International Conference on Communications (ICC)*, 2015, pp. 1304–1309.
- [17] R. Di Taranto, S. Muppisetty, R. Raulefs, D. Slock, T. Svensson, and H. Wymeersch, "Location-aware communications for 5G networks: How location information can improve scalability, latency, and robustness of 5G," *IEEE Signal Processing Magazine*, vol. 31, no. 6, pp. 102–112, 2014.
- [18] N. Garcia, H. Wymeersch, E. G. Ström, and D. Slock, "Location-aided mm-wave channel estimation for vehicular communication," in *17th International Workshop on Signal Processing Advances in Wireless Communications*. IEEE, 2016, pp. 1–5.
- [19] J. C. Aviles and A. Kouki, "Position-aided mm-wave beam training under NLOS conditions," *IEEE Access*, vol. 4, pp. 8703–8714, 2016.
- [20] F. Maschietti, D. Gesbert, P. de Kerret, and H. Wymeersch, "Robust location-aided beam alignment in millimeter wave massive MIMO," *arXiv preprint arXiv:1705.01002*, 2017.
- [21] T. Nitsche, C. Cordeiro, A. B. Flores, E. W. Knightly, E. Perahia, and J. C. Widmer, "IEEE 802.11 ad: directional 60 GHz communication for multi-Gigabit-per-second wi-fi," *IEEE Communications Magazine*, vol. 52, no. 12, pp. 132–141, 2014.
- [22] J. Wang, Z. Lan, C.-S. Sum, C.-W. Pyo, J. Gao, T. Baykas, A. Rahman, R. Funada, F. Kojima, I. Lakkis et al., "Beamforming codebook design and performance evaluation for 60GHz wideband WPANs," in *IEEE 70th Vehicular Technology Conference Fall*, 2009, pp. 1–6.

⁶Contrary to [24], we have not assumed that $\|\mathbf{a}_{\text{Tx}}(\theta)\| = \|\mathbf{a}_{\text{Rx}}(\phi)\| = 1$.

- [23] J. G. Andrews, T. Bai, M. N. Kulkarni, A. Alkhateeb, A. K. Gupta, and R. W. Heath, "Modeling and analyzing millimeter wave cellular systems," *IEEE Transactions on Communications*, vol. 65, no. 1, pp. 403–430, 2017.
- [24] A. Shahmansoori, G. E. Garcia, G. Destino, G. Seco-Granados, and H. Wymeersch, "5G position and orientation estimation through millimeter wave MIMO," in *GLOBECOM 2015*. IEEE, 2015, pp. 1–6.
- [25] H. L. Van Trees, *Detection, estimation, and modulation theory*. John Wiley & Sons, 2004.
- [26] C. Zhang, D. Guo, and P. Fan, "Tracking angles of departure and arrival in a mobile millimeter wave channel," in *2016 IEEE International Conference on Communications (ICC)*, pp. 1–6.
- [27] J. Palacios, D. De Donno, and J. Widmer, "Tracking mm-wave channel dynamics: Fast beam training strategies under mobility," in *2017 Conference on Computer Communications (INFOCOM)*. IEEE, pp. 1–9.
- [28] J. Bae, S. H. Lim, J. H. Yoo, and J. W. Choi, "New beam tracking technique for millimeter wave-band communications," *arXiv preprint arXiv:1702.00276*, 2017.
- [29] R. Méndez-Rial, C. Rusu, N. González-Prelcic, A. Alkhateeb, and R. W. Heath, "Hybrid mimo architectures for millimeter wave communications: Phase shifters or switches?" *IEEE Access*, vol. 4, pp. 247–267, 2016.
- [30] Z. Abu-Shaban, X. Zhou, T. Abhayapala, G. Seco-Granados, and H. Wymeersch, "Error bounds for uplink and downlink 3d localization in 5g mmwave systems," *arXiv preprint arXiv:1704.03234*, 2017.
- [31] M. S. Lobo, L. Vandenberghe, S. Boyd, and H. Lebrecht, "Applications of second-order cone programming," *Linear algebra and its applications*, vol. 284, no. 1, pp. 193–228, 1998.
- [32] S. Boyd and L. Vandenberghe, *Convex optimization*. Cambridge university press, 2004.
- [33] M. Grant, S. Boyd, and Y. Ye, "CVX: Matlab software for disciplined convex programming," 2008.
- [34] MOSEK ApS, "The MOSEK optimization toolbox for MATLAB manual, version 7.1 (revision 51)," <http://mosek.com>, (accessed on March 20, 2016).
- [35] J.-A. Tsai, R. M. Buehrer, and B. D. Woerner, "BER performance of a uniform circular array versus a uniform linear array in a mobile radio environment," *IEEE Transactions on Wireless Communications*, vol. 3, no. 3, pp. 695–700, 2004.
- [36] E. Bashan, A. J. Weiss, and B.-S. Yaakov, "Estimation near "zero information" points: angle-of-arrival near the endfire," *IEEE Transactions on Aerospace and Electronic Systems*, vol. 43, no. 4, pp. 1250–1264, 2007.
- [37] P. Stoica and A. Nehorai, "MUSIC, maximum likelihood, and Cramer-Rao bound," *IEEE Transactions on Acoustics, Speech, and Signal Processing*, vol. 37, no. 5, pp. 720–741, 1989.
- [38] B. Recht, M. Fazel, and P. A. Parrilo, "Guaranteed minimum-rank solutions of linear matrix equations via nuclear norm minimization," *SIAM review*, vol. 52, no. 3, pp. 471–501, 2010.
- [39] M. Fazel, H. Hindi, and S. P. Boyd, "A rank minimization heuristic with application to minimum order system approximation," in *American Control Conference, 2001*, vol. 6. IEEE, 2001, pp. 4734–4739.
- [40] G. H. Golub and C. F. Van Loan, *Matrix computations*. JHU Press, 2012, vol. 3.
- [41] I. Olkin and A. W. Marshall, *Inequalities: theory of majorization and its applications*. Academic press, 1979, vol. 143.
- [42] R. B. Bendel and M. R. Mickey, "Population correlation matrices for sampling experiments," *Communications in Statistics-Simulation and Computation*, vol. 7, no. 2, pp. 163–182, 1978.
- [43] P. I. Davies and N. J. Higham, "Numerically stable generation of correlation matrices and their factors," *BIT Numerical Mathematics*, vol. 40, no. 4, pp. 640–651, 2000.
- [44] H.-H. Lee and Y.-C. Ko, "Low complexity codebook-based beamforming for MIMO-OFDM systems in millimeter-wave WPAN," *IEEE Transactions on Wireless Communications*, vol. 10, no. 11, pp. 3607–3612, 2011.
- [45] L. C. Godara and A. Cantoni, "Uniqueness and linear independence of steering vectors in array space," *The Journal of the Acoustical Society of America*, vol. 70, no. 2, pp. 467–475, 1981.
- [46] H. Gazzah and K. Abed-Meraim, "Optimum ambiguity-free directional and omnidirectional planar antenna arrays for DOA estimation," *IEEE Transactions on signal processing*, vol. 57, no. 10, pp. 3942–3953, 2009.
- [47] V. Venkateswaran, F. Pivitt, and L. Guan, "Hybrid RF and digital beamformer for cellular networks: Algorithms, microwave architectures, and measurements," *IEEE Transactions on Microwave Theory and Techniques*, vol. 64, no. 7, pp. 2226–2243, 2016.
- [48] D. G. Manolakis, V. K. Ingle, and S. M. Kogon, *Statistical and adaptive signal processing: spectral estimation, signal modeling, adaptive filtering, and array processing*. McGraw-Hill Boston, 2000.